Journal of Thermal Analysis and Calorimetry, Vol. 91 (2008) 3, 855–860

THERMAL ANALYSIS OF SMITHSONITE AND HYDROZINCITE

M. C. Hales and R. L. Frost[*]

Inorganic Materials Research Program, School of Physical and Chemical Sciences, Queensland University of Technology, GPO Box 2434, Brisbane Queensland 4001, Australia

Thermogravimetric analysis of synthetic smithsonite and hydrozincite, two secondary minerals of zinc, was used to determine their relative thermal stability. Thermal decomposition of smithsonite occurs at 293°C and hydrozincite at 220°C showing that the carbonate mineral is more stable than the hydroxy-carbonate mineral hydrozincite. Hot stage Raman spectroscopy confirms the decomposition of smithsonite and hydrozincite by 300 and 250°C, respectively. Thermogravimetry shows that a small amount of hydrozincite is formed during the synthesis of smithsonite. No evidence is found for the separate loss of the carbonate and hydroxyl units from hydrozincite.

Keywords: *aurichalcite, hydrozincite, smithsonite, TG-MS, thermal analysis, thermogravimetric analysis*

Introduction

Smithsonite is naturally occurring zinc carbonate [1]. It is hexagonal with point group 3 bar 2/m. Carbonates with intermediate sized divalent cations normally crystallise in the calcite structure [2]. Those with larger cations have an aragonite type structure. Hydrozincite $Zn_5(CO_3)_2(OH)_6$, a mineral formed in the oxidised zones of zinc deposits, is often found as masses or crusts and is often not readily observed and may be confused with other minerals such as calcite [1]. The mineral is often associated with other secondary minerals such as smithsonite, hemimorphite, aurichalcite [1]. Hydrozincite is not commonly found as a crystalline material. Some lathe-like or bladed crystals may be uncommonly found. The mineral is flattened on and elongated on [3] with pointed terminations up to 6 mm in length. The mineral is monoclinic with point group 2/m [4–6]. Some considerations of the stacking in the crystals have been made [5].

Of the secondary minerals of zinc only two minerals are known namely smithsonite and hydrozincite. The formation of these minerals is controlled by the partial pressure of CO_2 [7, 8]. According to the equation for the formation of hydrozincite $5ZnO(s)+2CO_2(g)\leftrightarrow Zn_5(CO_3)_2(OH)_6(s)$ with $\log K=10.32$ [7]. Thus ZnO is unstable with respect to hydrozincite at partial pressures above $10^{-5.16}$. If the partial pressure of CO_2 increases above $10^{-1.41}$ smithsonite formation is favoured according to the reaction $Zn_5(CO_3)_2(OH)_6(s)+3CO_2(g)\leftrightarrow 5ZnCO_3(s)+3H_2O(g)$. These results provide implications for the relative stability of hydrozincite and smithsonite. Thus zincite (ZnO) is a rare mineral and smithsonite is only stable at elevated CO_2 partial pressures. The partial pressure range for the stability of hydrozincite according to Williams is limited and no doubt this accounts for the rarity of the mineral in nature [8]. The mineral can be readily synthesised in the laboratory and is often found in corrosion products of zinc [3, 9, 10]. In the presence of tenerite (CuO) the formation of malachite and/or azurite is favoured at the expense of hydrozincite [8]. Often the assemblage malachite-hydrozincite-hydrocerrusite is the stable system at 1 atmosphere CO_2 pressure.

Raman spectroscopy has proven very useful for the study of minerals [11–13]. Indeed Raman spectroscopy has proven most useful for the study of diagenetically related minerals such as carbonates and hydroxycarbonate [14–18]. Some previous studies have been undertaken by the authors using Raman spectroscopy to study complex secondary minerals formed by crystallisation from concentrated sulphate solutions [12–21]. Further hot stage Raman spectroscopy is most useful for the study of the thermal decomposition of minerals [22–27]. Thermal analysis has proven most useful for the analysis of the thermal decomposition of minerals [28–40]. The aim of this paper is to present the thermal analysis of synthetic smithsonite and hydrozincite supported by hot stage Raman spectroscopy and to discuss the TG-MS from a structural point of view. The paper is a part of systematic studies of vibrational spectra of minerals of secondary origin in the oxide supergene zone and their synthetic analogs.

* Author for correspondence: r.frost@qut.edu.au

1388–6150/$20.00

Akadémiai Kiadó, Budapest, Hungary
Springer, Dordrecht, The Netherlands

Experimental

Minerals

Synthesis of hydrozincite

Three different synthesis techniques were trialled for the synthesis of hydrozincite. The first involved weighing out equimolar amounts of the zinc(II) salt and the bi-carbonate salt, dissolving in a minimum volume of deionised water. The two zinc salts used in the experiment were zinc chloride ($ZnCl_2$) and zinc nitrate ($Zn(NO_3)_2$). Sodium hydrogen carbonate ($NaHCO_3$) was the source of the carbonate ion used for the experiments.

The following chemical reaction occurs with the reaction generating an atmosphere of CO_2.

$$5ZnCl_2(s)+10NaHCO_3(soln)\leftrightarrow Zn_5(CO_3)_2(OH)_6(s)+8CO_2(g)+10NaCl(soln)+2H_2O$$

Smithsonite is formed according to the following reaction:

$$ZnCl_2(soln)+2NaHCO_3(soln)\leftrightarrow ZnCO_3(s)+CO_2(g)+2NaCl(soln)+H_2O$$

Whether hydrozincite or smithsonite is obtained depends upon the partial pressure of CO_2.

The second experiment involved a similar process of mixing the reactants but at a controlled rate using a peristaltic pump system operating at 10 cm min^{-1}. The pH of the reaction was monitored but remained essentially constant at pH=7.2.

The following alternative reaction is envisaged for the formation of smithsonite:

$$Zn_5(CO_3)_2(OH)_6(s)+3CO_2(g)\leftrightarrow 5ZnCO_3(s)+3H_2O(g)$$

The third synthesis method involved hydrothermally treating some of the products from the previous two methods in a hydrothermal bomb at 100°C for 48 h with adequate washing of the products after removal from the bomb. Washing was deemed to be complete when the wash water no longer give a positive silver chloride test, indicating free chloride ions were removed. All of the samples were then washed and dried with ethanol and were placed in an oven at 80°C to dry thoroughly.

From the XRD analysis, it was found that there were some impurities of another synthetic mineral found in the samples that had both used zinc chloride and had then been hydro-thermally treated. It can be seen that hydrothermal treatment actually promotes the formation of this synthetic mineral identified as simonkolleite, a zinc chloride hydroxide hydrate mineral with the formula of $Zn_5(OH)_8Cl_2H_2O$. It is apparent that if the sample was synthesised using the $ZnCl_2$ and then hydro-thermally treated, the carbonate yield decreased significantly thereby increasing the yield of simonkolleite.

Methods

X-ray diffraction

XRD analyses were performed on a PANalytical X'Pert PRO® X-ray diffractometer (radius: 240.0 mm). Incident X-ray radiation was produced from a line focused PW3373/10 Cu X-ray tube, operating at 45 kV and 35 mA. The incident beam passed through a 0.04 rad, Soller slit, a 1/2° divergence slit, a 15 mm fixed mask and a 1° fixed anti scatter slit. After interaction with the sample, the diffracted beam was detected by an X'Celerator RTMS detector fitted to a graphite post-diffraction monochrometer. The detector was set in scanning mode, with an active length of 2.022 mm. Samples were analysed utilising Bragg–Brentano geometry over a range of 3–75° 2θ with a step size of 0.02° 2θ, with each step measured for 200 s.

Thermal analysis

Thermal decomposition of the zinc carbonates was carried out in a TA® Instruments incorporated high-resolution thermogravimetric analyzer (series Q500) in a flowing nitrogen atmosphere (60 cm^3 min^{-1}). Approximately 35 mg of sample underwent thermal analysis, with a heating rate of 5°C min^{-1}, and high resolution, to 1000°C. With the heating program of the instrument the furnace temperature was regulated precisely to provide a uniform rate of decomposition in the main decomposition stage. The TG instrument was coupled to a Balzers (Pfeiffer) mass spectrometer for gas analysis. Only water vapour, carbon dioxide and oxygen were analyzed.

Raman spectroscopy

The crystals of smithsonite or hydrozincite were placed and oriented on the stage of an Olympus BHSM microscope, equipped with 10× and 50× objectives and part of a Renishaw 1000 Raman microscope system, which also includes a monochromator, a filter system and a charge coupled device (CCD). Raman spectra were excited by a HeNe laser (633 nm) at a resolution of 2 cm^{-1} in the range between 100 and 4000 cm^{-1}. Repeated acquisition using the highest magnification was accumulated to improve the signal to noise ratio. Spectra were calibrated using the 520.5 cm^{-1} line of a silicon wafer. In order to ensure that the correct spectra are obtained, the incident excitation radiation was scrambled. Previous studies by the authors provide more details of the experimental technique [11, 12, 15, 17, 41–47].

Spectra at elevated temperatures were obtained using a Linkam thermal stage (Scientific Instruments Ltd., Waterfield, Surrey, England). Spectral manipulation such as baseline adjustment, smoothing and normalisation was performed using the GRAMS® software package (Galactic Industries Corporation, Salem, NH, USA).

Results and discussion

X-ray diffraction

In certain conditions as detailed above synthetic smithsonite or synthetic hydrozincite is produced. Further an impurity of simonkolleite with hydrozincite may be synthesised depending upon the starting materials. The conditions for the formation of simonkolleite are similar to that for hydrozincite. It was found that if zinc chloride was used in the synthesis and the sample was hydrothermally treated, a significant yield of simonkolleite was produced. The sample was still a mixed phase of simonkolleite and hydrozincite. It is also interesting that when smithsonite is formed, simonkolleite is not. The XRD patterns together with standard XRD reference patterns of synthetic smithsonite and hydrozincite are shown in Fig. 1. Clearly the pure hydrozincite and smithsonite phases were synthesised as single phases.

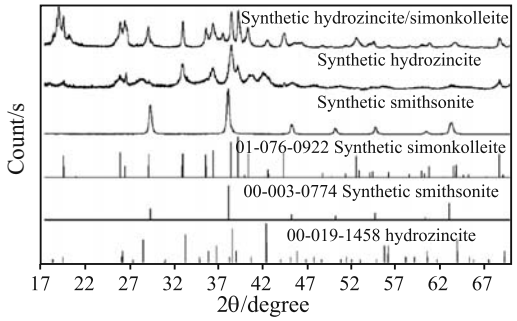

Fig. 1 X-ray diffraction patterns of synthetic hydrozincite and smithsonite together with the standard reference patterns

Thermogravimetric and ion current analysis

Thermal analysis of smithsonite

The thermal analysis of smithsonite is reported in Fig. 2a. The ion current curves for the gas evolution from the thermal decomposition of smithsonite are shown in Fig. 2b. The thermogravimetric pattern shows a slow mass loss starting at 175°C with two steps at 235 and 293°C with mass losses of 2.98 and 29.16%. The total mass loss from 175 to 330°C is 33.19%. A further mass loss of 2.09% is observed until a constant mass is obtained. This makes a total of 35.2% which is identical to the predicted mass loss from smithsonite according to the reaction:

$$ZnCO_3 \rightarrow ZnO + CO_2$$

The DTG curve shows a small peak at 235°C and a large sharp peak at 265°C. The ion current curves for m/z=44 corresponding to the mass of CO_2 shows two maxima at 226 and 265°C. These values correspond to the peaks in the DTG patterns. m/z ion current curves for 16, 17 and 18 are shown. These curves

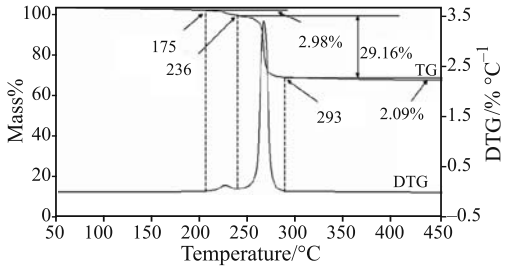

Fig. 2a Thermogravimetric analysis of smithsonite

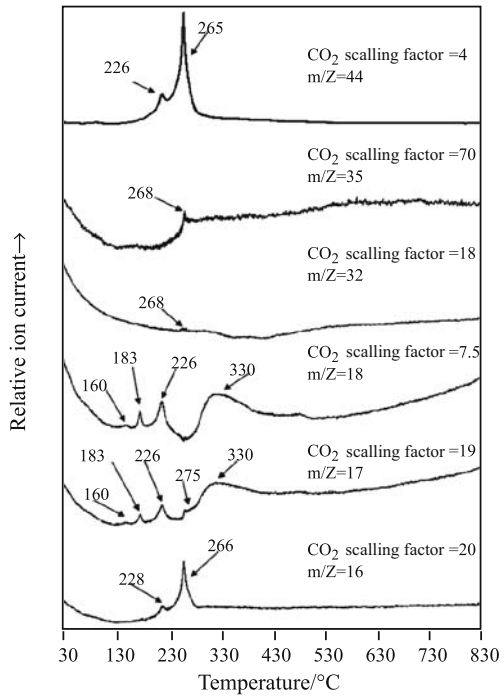

Fig. 2b Ion current curves for the evolved gases in the thermal decomposition of smithsonite

show a loss of H_2O and OH units at 160, 183, 226 and 330°C. It should be noted that the scaling factors for ion current curves is very high. Hence only small amounts of OH or H_2O are released. One possibility is that these ion current curves are attributable to a trace of hydrozincite in the synthesised smithsonite. This is in some ways not unexpected.

Thermal analysis of hydrozincite

The thermogravimetric and differential thermogravimetric analyses are shown in Fig. 3a. In the TG curves mass loss starts at around 156°C and is complete by 440°C. The main mass loss occurs at 220°C with a mass loss of 22%. A mass loss of 3.14% is observed between ~239 and 441°C. The theoretical mass loss may be calculated according to the equation:

$$Zn_5(CO_3)_2(OH)_6 \rightarrow 5ZnO + 2CO_2 + 3H_2O$$

This value equals 34.72%. The theoretical mass loss of CO_2 is 18.64% and for OH units is 16.08%. The

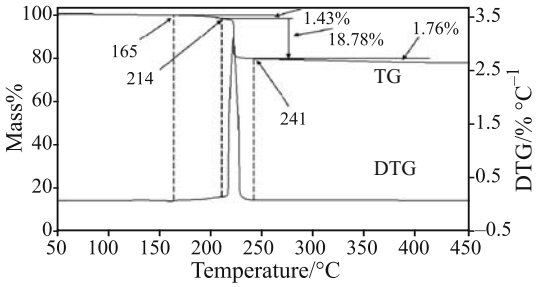

Fig. 3a Thermogravimetric analysis of hydrozincite

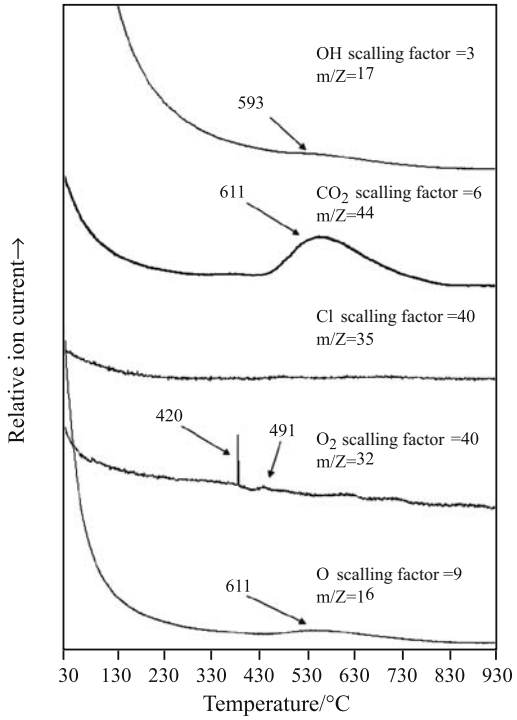

Fig. 3b Ion current curves for the evolved gases in the thermal decomposition of hydrozincite

thermal analysis patterns do not provide any evidence for the OH and CO_2 units being lost separately. The observed total mass loss is 21.97%. The difference is accounted for by the loss due to the formation of a second phase namely simonkolleite. The ion current curves which measure the gas evolution are shown in Fig. 3b. This figure shows the temperature of the thermal decomposition as measured by gas evolution as 220°C. Other gas evolution steps are observed at 48 and 134°C.

Hot stage Raman spectroscopy

The free ion, CO_3^{2-} with D_{3h} symmetry exhibits four normal vibrational modes; a symmetric stretching vibration (ν_1), an out-of-plane bend (ν_2), a doubly degenerate asymmetric stretch (ν_3) and another doubly degenerate bending mode (ν_4). The symmetries of these modes are $A'_2(R)+A''_2(IR)+E'(R,IR)+E''(R,IR)$ and occur at 1063, 879, 1415 and 680 cm^{-1}, respectively. Generally, strong Raman modes appear around 1100 cm^{-1} due to the symmetric stretching vibration (ν_1), of the carbonate groups, while intense IR and weak Raman peaks near 1400 cm^{-1} are due to the antisymmetric stretch (ν_3). Infrared modes near 800 cm^{-1} are derived from the out-of-plane bend (ν_2). Infrared and Raman modes around 700 cm^{-1} region are due to the in-plane bending mode (ν_4). This mode is doubly degenerate for undistorted CO_3^{2-} groups. As the carbonate groups become distorted from regular planar symmetry, this mode splits into two components. Infrared and Raman spectroscopy provide sensitive test for structural distortion of CO_3^{2-}.

The hot stage Raman spectra of smithsonite are shown in Fig. 4. Vibrational spectroscopic studies of carbonate minerals have been undertaken over an extended period of time [48–50]. Adler and Kerr showed that differences in the infrared absorption spectra of carbonates were a function of cation size [48]. Raman studies also have been forthcoming but not recently [51–53]. Farmer reported the vibrational wavenumbers of calcite structured minerals (Table 12, IX page 239) [2]. In this table the band positions for smithsonite were listed as 1093 cm^{-1} (ν_1 symmetric stretching mode), 1412 and 1440 cm^{-1} (ν_3 antisymmetric stretching mode), 870 cm^{-1} (ν_2 in-plane bending mode), 733 and 743 cm^{-1} (ν_4 out of plane bending mode) with lattice modes at 307, 200, 165 cm^{-1}. Some variation of band positions is found in the literature.

An intense Raman band at 1091 cm^{-1} is observed for all of the samples studied. This band is attributed to the ν_1 (CO_3^{2-}) symmetric stretching mode. The band is observed in all the spectra up to 300°C but the intensity of the band is lost after this temperature. The band shows a slight red shift and is observed at 1089.7 cm^{-1} at 300°C. After 300°C, the spectrum is completely different and is that of ZnO. In the TG curves the smithsonite decomposed at 265°C. The Raman spectra are in harmony with this observation. The Raman bands at 1405 cm^{-1} is attributed to ν_3 (CO_3^{2-}) antisymmetric stretching mode. This band shifts to 1395.6 cm^{-1} at 300°C. Farmer reports two bands in this spectral region for smithsonite at 1412 and 1440 cm^{-1} [2]. For smithsonite only a single band at 728 cm^{-1} is observed assigned to the carbonate ν_4 in phase bending modes. This band is present in all the spectra and the intensity is lost above 300°C. The ν_2 bending mode for carbonates varies from around 890 to 850 cm^{-1}. For smithsonite Farmer reported an infrared band at 870 cm^{-1} [2]. In this work no Raman bands are observed for the synthetic smithsonite in this position. The band is only observed in the higher temperature spectra for example at 250°C.

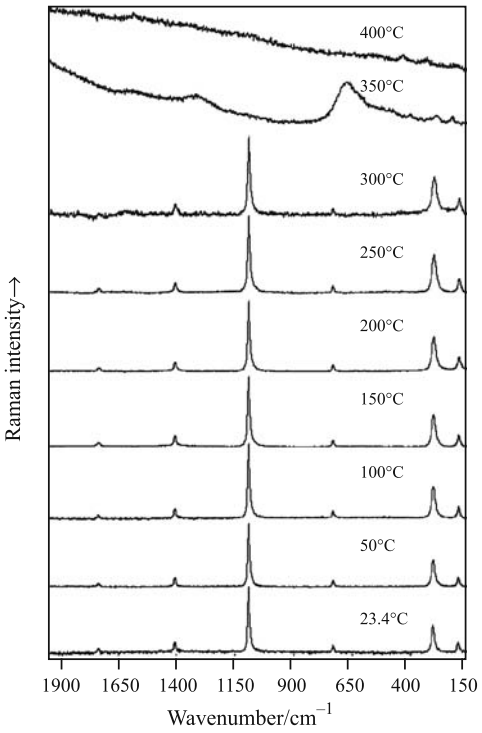

Fig. 4 Raman spectroscopy of smithsonite from ambient temperature to 400°C

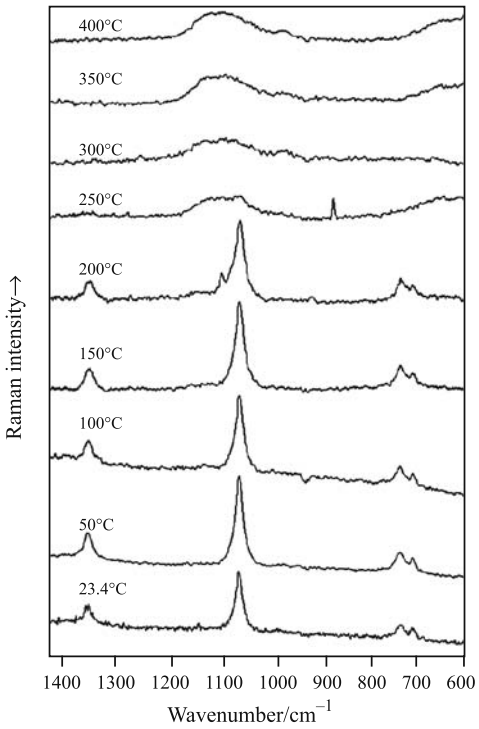

Fig. 5 Raman spectroscopy of hydrozincite from ambient temperature to 400°C

The hot stage Raman spectra of synthetic hydrozincite are shown in Fig. 5. The Raman spectrum of synthetic hydrozincite shows an intense sharp band at 1062 cm^{-1}. The intensity of this band is lost by 250°C. The band shifts to 1057.8 cm^{-1} at 300°C. In the 150°C spectrum a shoulder at 1092 cm^{-1} is observed. The band is more prominent in the 200°C spectrum, observed at 1095 cm^{-1}. This band may be due to the presence of smithsonite and this observation offers a mechanism for the thermal decomposition of hydrozincite. It is possible the hydrozincite converts to smithsonite before the smithsonite is decomposed. However such a step is not observed in the TG results which show the carbonate and OH units are lost simultaneously. For synthetic hydrozincite bands at 1545 and 1367 cm^{-1} are found and are ascribed to OH deformation and the ν_3 (CO_3^{2-}) antisymmetric stretching modes. Intensity in these bands is lost by 250°C. A very low intensity Raman band is observed at 850 cm^{-1} assigned to the ν_2 bending mode. This band is not observed in the smithsonite spectrum. The band is more prominent in the 200°C spectrum. This may indicate the symmetry of the carbonate anion is reduced upon heating of the hydrozincite.

Two Raman bands are observed at 703 and 728 cm^{-1} assigned to the ν_4 bending modes. Interestingly Farmer (based upon the work of Moenke [50] reported two infrared bands for hydrozincite at 738 and 710 cm^{-1} [2]. Farmer also reported only a single Raman band for smithsonite at 733 cm^{-1}.

Conclusions

Of the secondary minerals of zinc only two minerals are known namely smithsonite and hydrozincite and their formation is controlled by the partial pressure of CO_2 according to the reactions

$$5ZnO(s)+2CO_2(g)+3H_2O \leftrightarrow Zn_5(CO_3)_2(OH)_6(s)$$

and

$$Zn_5(CO_3)_2(OH)_6(s)+3CO_2(g) \leftrightarrow 5ZnCO_3(s)+3H_2O(g)$$

The stability of these minerals has been determined by a combination of thermogravimetry and hot stage Raman spectroscopy.

TG analysis shows that synthetic smithsonite decomposes at 265°C. A second decomposition step is observed at 228°C and is attributed to a synthetic hydrozincite impurity in the synthetic smithsonite. A total mass loss for synthetic smithsonite of 35.28 % which is in excellent agreement with the theoretical mass loss of 35.2%. Hot stage Raman spectroscopy shows that the Raman spectrum of smithsonite is lost by 300°C, in harmony with the TG-MS results. The thermal decomposition of hydrozincite occurs at 220°C with an experimental mass loss of 21.97%. Hot stage Raman spectroscopy of hydrozincite shows the mineral decomposes by 250°C in agreement with the thermal analysis results.

Acknowledgements

The financial and infrastructure support of the Queensland University of Technology Inorganic Materials Research Program of the School of Physical and Chemical Sciences is gratefully acknowledged. The Australian Research Council (ARC) is thanked for funding the Thermal Analysis Facility.

References

1 J. W. Anthony, R. A. Bideaux, K. W. Bladh and M. C. Nichols, Handbook of Mineralogy, Mineral Data Publishing, Tiscon, Arizona, USA 2003.
2 V. C. Farmer, Mineralogical Society Monograph 4: The Infrared Spectra of Minerals, 1974.
3 M. Bouchard and D. C. Smith, Asian Chem. Lett., 5 (2001) 157.
4 M. M. Harding, B. M. Kariuki, R. Cernik and G. Cressey, Acta Crystallogr., Section B: Struct. Sci., B50 (1994) 673.
5 W. Zabinski, Can. Mineral., 8 (1966) 649.
6 S. Ghose, Acta Cryst., 17 (1964) 1051-1057.
7 A. K. Alwan and P. A. Williams, Transition Metal Chemistry (Dordrecht, Netherlands), 4 (1979) 128.
8 P. A. Williams, Oxide Zone Geochemistry, Ellis Horwood Ltd. Chichester, West Sussex, England 1990.
9 J. L. Jambor, Can. Mineral., 8 (1964) 92.
10 F. Zhu, D. Persson and D. Thierry, Corrosion (Houston, TX, United States), 57 (2001) 582.
11 R. L. Frost, S. J. Palmer, J. M. Bouzaid and B. J. Reddy, J. Raman Spectrosc., 38 (2007) 68.
12 R. L. Frost, D. A. Henry, M. L. Weier and W. Martens, J. Raman Spectrosc.. 37 (2006) 722.
13 R. L. Frost, A. W. Musumeci, J. T. Kloprogge, M. O. Adebajo and W. N. Martens, J. Raman Spectrosc., 37 (2006) 733.
14 R. L. Frost, J. Cejka, M. Weier and W. N. Martens, J. Raman Spectrosc., 37 (2006) 879.
15 R. L. Frost, M. L. Weier, J. Cejka and J. T. Kloprogge, J. Raman Spectrosc., 37 (2006) 585.
16 R. L. Frost, J. Cejka, M. L. Weier and W. Martens, J. Raman Spectrosc., 37 (2006) 538.
17 R. L. Frost, M. L. Weier, B. J. Reddy and J. Cejka, J. Raman Spectrosc., 37 (2006) 816.
18 R. L. Frost, M. L. Weier, W. N. Martens, J. T. Kloprogge and J. Kristóf, J. Raman Spectrosc., 36 (2005) 797.
19 R. L. Frost, J. Raman Spectrosc., 37 (2006) 910.
20 R. L. Frost, R. -A. Wills, M. L. Weier and W. Martens, J. Raman Spectrosc., 36 (2005) 435.
21 R. L. Frost, A. W. Musumeci, W. N. Martens, M. O. Adebajo and J. Bouzaid, J. Raman Spectrosc., 36 (2005) 925.
22 R. L. Frost and M. L. Weier, J. Therm. Anal. Cal., 75 (2004) 277.
23 R. L. Frost, K. Erickson and M. Weier, J. Therm. Anal. Cal., 77 (2004) 851.
24 R. L. Frost, S. J. Mills and K. L. Erickson, Thermochim. Acta, 419 (2004) 109.
25 R. L. Frost, M. L. Weier and W. Martens, J. Therm. Anal. Cal., 82 (2005) 373.
26 R. L. Frost, M. L. Weier, W. Martens and S. Mills, J. Mol. Struct., 752 (2005) 178.
27 R. L. Frost, A. W. Musumeci, J. Bouzaid, M. O. Adebajo, W. N. Martens and J. T. Kloprogge, J. Solid State Chem., 178 (2005) 1940.
28 J. Bouzaid and R. L. Frost, J. Therm. Anal. Cal., 89 (2007) 133.
29 J. M. Bouzaid, R. L. Frost and W. N. Martens, J. Therm. Anal. Cal., 89 (2007) 511.
30 J. M. Bouzaid, R. L. Frost, A. W. Musumeci and W. N. Martens, J. Therm. Anal. Cal., 86 (2006) 745.
31 R. L. Frost, J. M. Bouzaid, A. W. Musumeci, J. T. Kloprogge and W. N. Martens, J. Therm. Anal. Cal., 86 (2006) 437.
32 R. L. Frost, J. Kristóf, W. N. Martens, M. L. Weier and E. Horváth, J. Therm. Anal. Cal., 83 (2006) 675.
33 R. L. Frost, J. Kristóf, M. L. Weier, W. N. Martens and E. Horváth, J. Therm. Anal. Cal., 79 (2005) 721.
34 R. L. Frost, A. W. Musumeci, M. O. Adebajo and W. Martens, J. Therm. Anal. Cal., 89 (2007) 95.
35 R. L. Frost, A. W. Musumeci, J. T. Kloprogge, M. L. Weier, M. O. Adebajo and W. Martens, J. Therm. Anal. Cal., 86 (2006) 205.
36 R. L. Frost, M. L. Weier ad W. Martens, J. Therm. Anal. Cal., 82 (2005) 115.
37 R. L. Frost, R. -A. Wills, J. T. Kloprogge and W. Martens, J. Therm. Anal. Cal., 84 (2006) 489.
38 R. L. Frost, R. -A. Wills, J. T. Kloprogge and W. N. Martens, J. Therm. Anal. Cal., 83 (2006) 213.
39 A. W. Musumeci, G. G. Silva, W. N. Martens, E. R. Waclawik and R. L. Frost, J. Therm. Anal. Cal., 88 (2007) 885.
40 Y. Xi, W. Martens, H. He and R. L. Frost, J. Therm. Anal. Cal., 81 (2005) 91.
41 R. L. Frost, J. M. Bouzaid, W. N. Martens and B. J. Reddy, J. Raman Spectrosc., 38 (2007) 135.
42 R. L. Frost, J. Cejka and M. L. Weier, J. Raman Spectrosc., 38 (2007) 460.
43 R. L. Frost, M. L. Weier, P. A. Williams, P. Leverett and J. T. Kloprogge, J. Raman Spectrosc., 38 (2007) 574.
44 R. L. Frost, Anal. Chim. Acta, 517 (2004) 207.
45 R. L. Frost, J. T. Kloprogge and W. N. Martens, J. Raman Spectrosc., 35 (2004) 28.
46 R. L. Frost and M. L. Weier, J. Raman Spectrosc., 35 (2004) 299.
47 R. L. Frost, P. A. Williams, W. Martens, P. Leverett and J. T. Kloprogge, Am. Mineral., 89 (2004) 1130.
48 H. H. Adler and P. F. Kerr, American Mineral., 48 (1963) 124.
49 C. K. Huang and P. F. Kerr, American Mineral., 45 (1960) 311.
50 H. Moenke and W. Zabinski, Geologie (Berlin), 12 (1963) 1221.
51 W. P. Griffith, Nature (London, United Kingdom), 224 (1969) 264.
52 R. G. Herman, C. E. Bogdan and A. J. Sommer, Mater. Sci. Res., 19 (1985) 113.
53 W. P. Griffith, J. Chem. Soc. A: Inorg. Phys. Theoretical, (1970) 286.

Received: May 22, 2007
Accepted: September 5, 2007

DOI: 10.1007/s10973-007-8571-0